Proceedings of the IASS 2024 Symposium
Redefining the Art of Structural Design
August 26-30, 2024, Zurich Switzerland
Philippe Block, Giulia Boller, Catherine DeWolf,
Jacqueline Pauli, Walter Kaufmann (eds.)

Load-bearing test of a hybrid steel-concrete joint for discrete reticulated timber shell structures with six linear members

Žiga UNUK*

*University of Maribor, Faculty of Civil Engineering, Transportation Engineering and Architecture
Smetanova ulica 17, 2000 Maribor, Slovenia
ziga.unuk@um.si

Abstract

The article presents a load-bearing test of a spatial specimen with six linear glued laminated timber elements inclined to the horizontal plane and joined with a hybrid steel-concrete joint for discrete reticulated timber structures. The specimen itself can be considered as a small discrete reticulated structure. The core of the joint consists of a steel tube with concrete filling, where the contact face between the concrete infill and the steel tube allows (by design) the transfer of loads only through friction and compression contacts. Glued-in threaded rods connected the glued-laminated timber elements to the steel tube via a configuration of steel plates. The test specimen was loaded by a vertical force acting at the joint. The load was applied with a constant displacement increase. The article focuses on the experimental determination of the load-bearing capacity and stiffness of the studied structural elements. The specimen load-bearing capacity was limited by the glued-in threaded rod pull-out failure (rupture of timber on a nearly cylindrical surface near the glued-in threaded rod adhesive layer). The specimen behaved in a ductile manner. The concrete infill of the specimen remained undamaged even after testing. Experimental results were also evaluated with calculations of load-bearing capacity and stiffness.

Keywords: joint, discrete reticulated shell structures, timber, glued-in rods, concrete, steel, load-bearing test

1. Introduction

Gridshell structures, also called reticulated shell structures or space frame structures, stand out as significant engineering achievements, characterized by their unique spatial configurations and sophisticated structural engineering principles. As highlighted in [1], following a comprehensive literature review on gridshell structures, it is noted that existing examples of these structures can be categorized into three types: curved, actively curved, and discrete. While gridshell structures of the first two types are mostly made up of linear elements uninterrupted at the nodes, the discrete grid structures are made up of relatively shorter linear elements interrupted at the grid nodes and joined with special joint systems. The study [2] points to the disadvantage of discrete gridshell structures being the complex joints, which require the use of computer-aided manufacturing (CAM); however, this is an area where developments are rapid, as shown in [3]. Adequately designed and manufactured joints ensure discrete gridshell structures closely align to various surfaces' geometry.

Typical materials for gridshell structures are steel and timber. From an environmental point of view, it is generally preferable to use timber for buildings, as demonstrated by many studies (e.g. [4], [5]). However, steel plays a significant role in the joints of discrete gridshell structures, whose structural behavior depends mainly on the joints at the grid nodes. In discrete timber gridshell structures, the joints are usually made up of steel tubes. In order to increase the stiffness and load-bearing capacity of the joints, these steel tubes have relatively thick walls, sometimes with additional welded stiffener elements, which results in disproportionately large amounts of steel being used for the joints. In [6], it is estimated that the joints account for 15-40% of the self-weight weight of roof structures with larger spans (e.g.,

for stadia). Similar or even higher proportions can be attributed to gridshell structures, nevertheless, many studies in the field of gridshell structures deal with optimizing the shape of the joints and the consequent reduction of the mass of the joints (e.g. [7]). It would be more advantageous to minimize the thickness of the steel tube and replace it as much as possible with another cheaper material with a lower density and a lower environmental impact than steel – this description fits concrete.

According to [8], dowel-type joint and glued-in rod joint configurations are most commonly incorporated in the joints of glued-laminated timber gridshell structures. Furthermore, glued-in threaded rod joints are favored over dowel-type joints for their on-site assembly convenience. This paper, therefore, focuses on the structural behavior of a spatial specimen consisting of six glued-laminated timber (glulam) beams joined in one node with a hybrid steel-concrete joint. The core of the joint is a steel tube with concrete infill. A configuration of steel plates welded to the steel tube connects the steel tube with the glulam beams via glued-in threaded rods. The experimental determination of the load-bearing capacity and stiffness of the spatial specimen is first presented. A calculation model is also briefly presented to determine the load-bearing capacity and stiffness. Finally, the experimental and calculation results are compared.

2. Load-bearing test

A load-bearing test was performed on a spatial specimen with six linear glued-laminated timber elements (glulam beams) connected at one joint and inclined to the horizontal plane. The test specimen dimensions can be seen in Figure 1. The glulam beam cross-section was 20 cm wide and 36 cm high. The glulam beam strength class was GL24h.

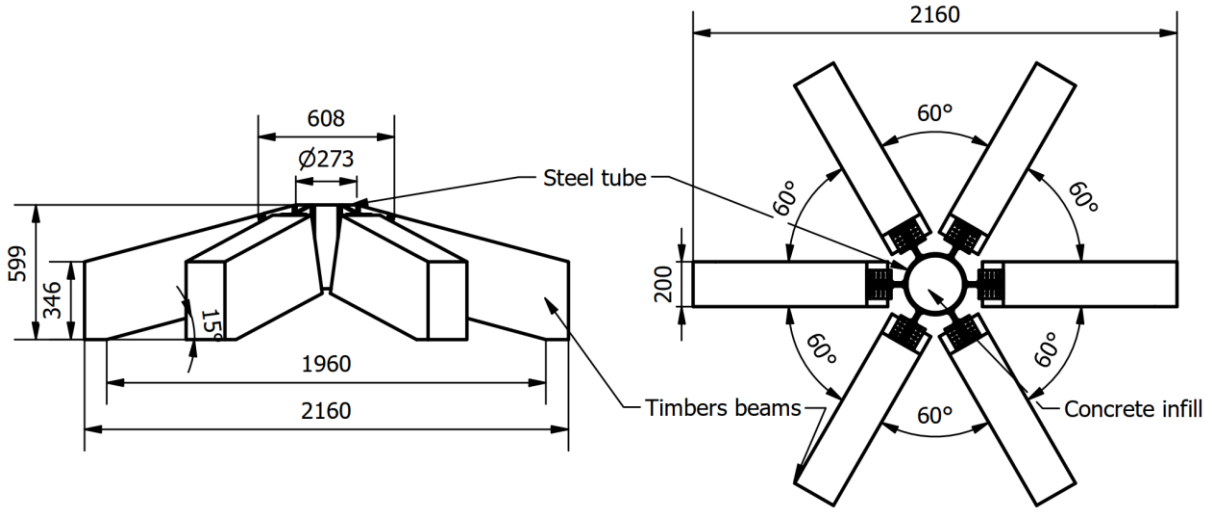

Figure 1: Test specimen dimensions in mm (left: front view; right: top view).

The core of the joint (Figure 2) is represented by a steel tube with an external diameter of 273 mm and a wall thickness of 10 mm. The height of the steel tube was about 373 mm. Multiple steel plates (interim and endplates) with a thickness of 15 mm were welded to the steel to connect the glulam beams to the joint. All welds were filled welds and had a weld leg size of 11 mm (or a throat thickness of about 7.5 mm). The strength class of all steel elements was S355. The steel tube was filled with a concrete of strength class C25/30 (according to the declaration of properties). The Barchip 48 [9] high-performance macro-synthetic polypropylene fibers, designed for structural reinforcement in precast, paving and flooring works [9], were added to the concrete mixture. 5 kg of the fibers was added per cubic meter of the concrete composition. The fibers can be classified as Class II fibers (according to the standard EN 14889-2 [10]), generally used where an increase in residual flexural strength is required. The concrete infill compressive, tensile and residual tensile strengths were experimentally assessed in [11].

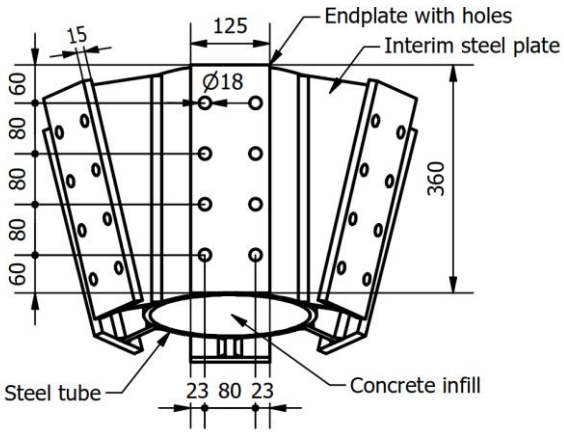

Figure 2: Joint – steel tube with concrete infill and welded steel interim and endplates (view direction perpendicular to one endplate, all dimensions in mm).

The connection between the glulam beam end face and the steel endplates was a bolted butt joint, more common in steel construction. The steel endplates had holes with a diameter of 18 mm, which were meant for receiving steel bolts with a nominal diameter of 16 mm. Counterbore holes with two different diameters and depths were drilled in the end faces of the glulam beams (Figure 3). The larger diameter hole (24 mm) was drilled to a depth of 50 mm and was intended for inserting a coupling nut, while the smaller diameter hole (18 mm) was drilled to a depth of 302 mm and was intended for inserting a threaded rod. The threaded rod length was chosen based on multiple experiment configurations (not presented in this paper). Eight bolts were needed to connect the steel endplates and the glulam beams. The bolts passed through the holes in the steel endplate and were bolted in the coupling nuts. For gluing the threaded rods and coupling nuts to the glulam beams, a two-component epoxy adhesive (Rothoblaas Xepox D) was used. The bolts, threaded rods and nuts were of strength class 8.8 or comparable.

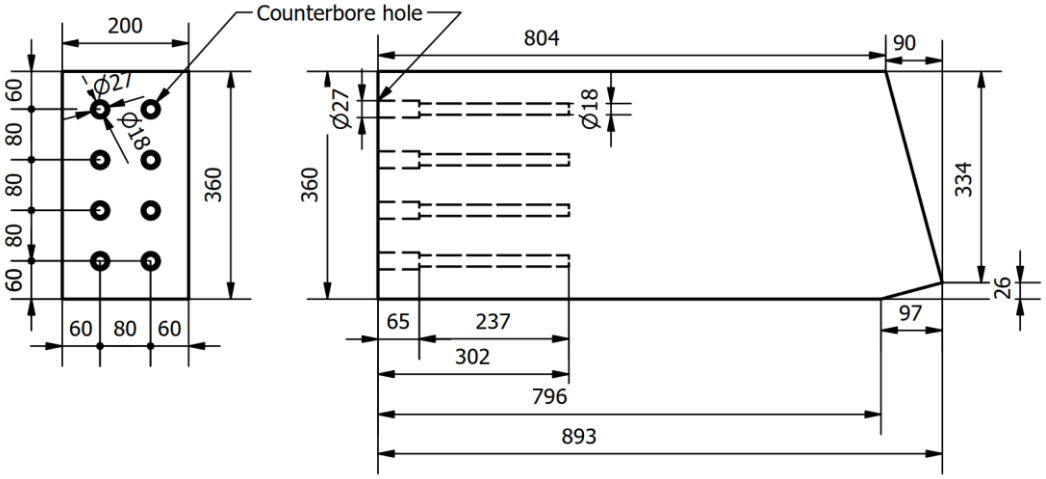

Figure 3: Glulam beam dimensions in mm (left: end cross-section; right: side view with displayed counterbore holes).

2.2 Test execution and results

The test was performed at The Slovenian National Building and Civil Engineering Institute. The specimen was loaded in the vertical direction (Figure 4). The load was introduced at the joint. A sandwich of steel plates and Teflon sheets was placed between the concrete-infilled steel tube and the load piston to disclose the load piston's possible impact on the joint's structural behavior and to distribute the load to the joint. Teflon sheets were also placed between the supported faces of the glulam beams

and the ground to minimize the contact friction. Consequently, the test specimen was only vertically supported.

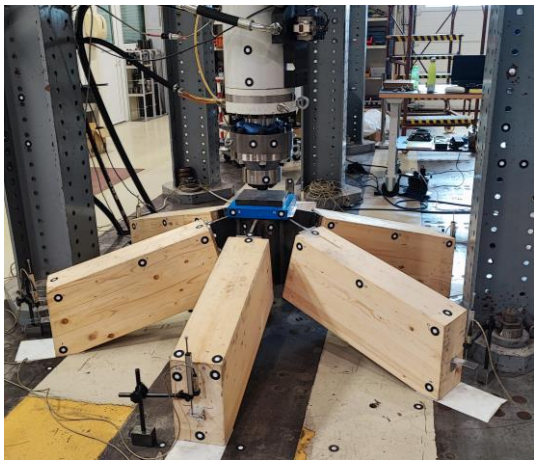

Figure 4: The load-bearing test configuration.

The loading of the specimen was displacement-controlled – the displacement increase rate was 0.05 mm/s. The displacement measurements were carried out using the optical measuring device ARAMIS SRX, which monitored several marked discrete points. Additionally, LVDT (Linear Variable Differential Transformer) displacement sensors were installed to monitor the vertical displacement at the supports. The vertical displacement was measured at the steel tube's outer surface, which was visible with the optical measuring device. The results of the load-bearing test are shown in the form of a load-displacement curve in Figure 5.

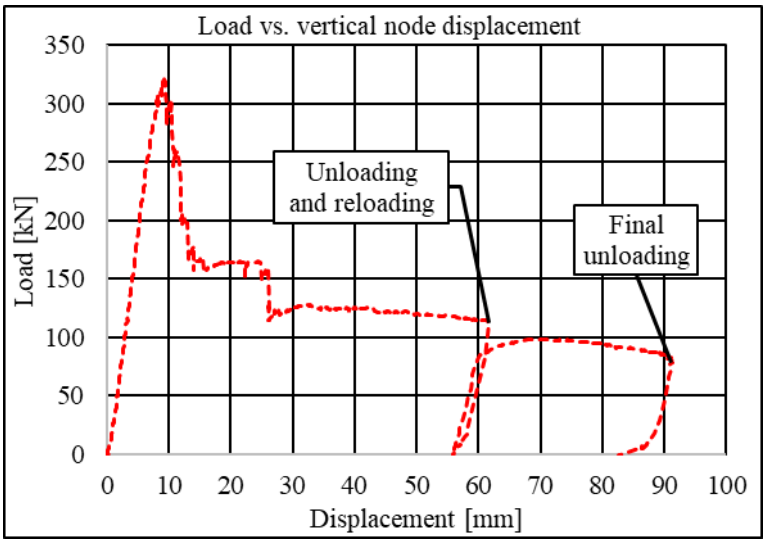

Figure 5: Load-bearing test results in the form of a load-displacement curve.

The test was carried out until a vertical displacement of about 90 mm was reached. Afterward, the specimen was unloaded (final unloading in Figure 5). The reason for stopping the test was a horizontal movement (sliding) of the test specimen. The test specimen was also unloaded and reloaded at a vertical displacement of about 60 mm to adjust the LVDT sensors to the deformed specimen shape. The load was already below 50 % of the maximum load reached during the load-bearing test.

After the initial settling phase (which can be considered up to a load of about 25 kN), the specimen's load-displacement behavior was nearly linear up to about 300 kN. By increasing the load and still prior to reaching the maximum load (about 324 kN at a vertical displacement of about 10 mm), the load even decreased a few times and increased again, which indicates the redistribution of the loads between the

glued-in threaded rods and/or between the glulam beams. The specimen's maximum load (load-bearing capacity) was limited by the pull-out of the glued-in threaded rods (the bottom ones in relation to the glulam beam cross-section). However, the specimen did not fail, as after reaching the maximum load, the load decreased relatively sharply to about 50 % of the maximum load when the load-displacement curve started to have a narrower slope. Even after reaching the maximum load, the load increased and decreased again at several vertical displacements. Therefore, the structural behavior of the specimen during the load-bearing test can be described as ductile. The load-bearing test resulted in three (out of six) glulam beams having heavily damaged glued-in threaded rod connections (Figure 6 (left)). The deformed glued-in threaded rod connection of one glulam beam is shown in Figure 6 (right), where it can be seen how the horizontal displacements of the connection cross-section linearly increased from the top to the bottom of the cross-section.

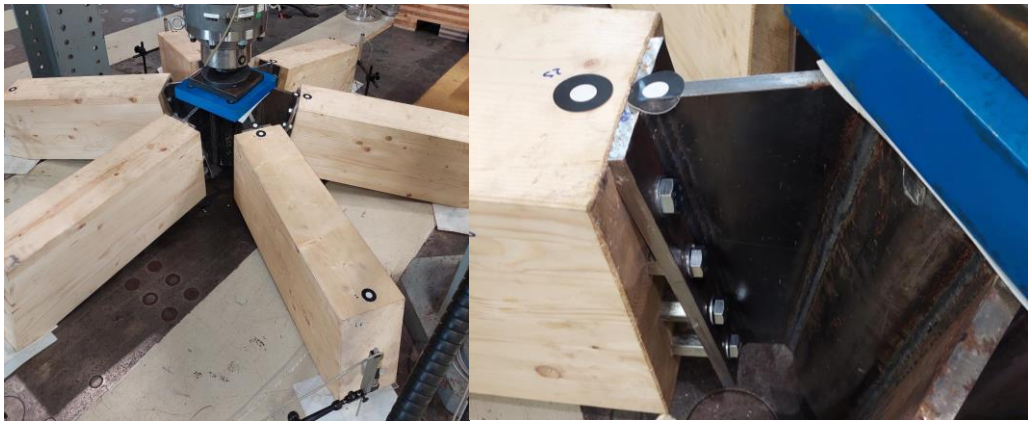

Figure 6: Test specimen after the load-bearing test (left: whole specimen; right: close-up view of the ruptured glued-in threaded rod connection of a single glulam beam.

The stiffness of the test specimen was evaluated on the interval between the load of 50 kN and 250 kN (on the initial loading part of the load-displacement curve). The stiffness was defined as the load and vertical displacement difference ratio. To disclose the support deformation effect, the vertical displacements at the glulam beams supports measured with the LVDT sensors were subtracted from the vertical displacement of the steel tube. The considered load and displacement values resulted in a stiffness of about 46 kN/mm (see Table 1).

Table 1: Load and displacement values considered for the stiffness calculation.

Load [kN]	Vertical displacement [mm]	Average support vertical displacement [mm]	Stiffness [kN/mm]
50	1.69	0.87	46.31
250	6.43	1.29	

An important insight from the load-bearing test was also that the load-bearing test did not result in any damage (noticeable cracks) of the concrete infill – during the performed load-bearing test the concrete infill (cylinder) was loaded in multiple transversal directions (in the pressure zone in the sense of bending moments applied on cross-sections).

3. Calculation of the stiffness and load-bearing capacity

The behavior of the proposed joint can be divided into two subproblems. The first is the behavior of the steel tube with the concrete infill, and the second is the behavior of the connection between the steel endplates and the glulam beams with the bolts, coupling nuts and glued threaded rods. For the rotational stiffness of the steel tube and concrete infill interaction, only the transmission of pressure contact forces between the steel tube and the concrete infill was considered. It was assumed that the steel tube wall acts as a beam and the neighboring interim steel plates act as fixed supports for the steel plate wall beam.

Two mechanisms were defined for simulating the contact behavior between the steel tube and the concrete infill. For the first mechanism, it was supposed that a bending moment acting on the steel tube wall acts as a force couple, a compression force (Figure 7 a) and a tensile force (Figure 7 b) acting on different steel tube wall parts. The steel tube and the concrete infill act as parallel springs for the compression force, while the concrete infill is not activated for the tension force. For the second mechanism, the steel tube wall, loaded by a bending moment, transfers the acting bending moment to the neighboring interim steel plates (acting as fixed supports) in the form of internal static quantities of bending and torsional moments (Figure 7 c). In the present case, the neighboring interim steel plates formed angles (α_1 and α_2) of 60°.

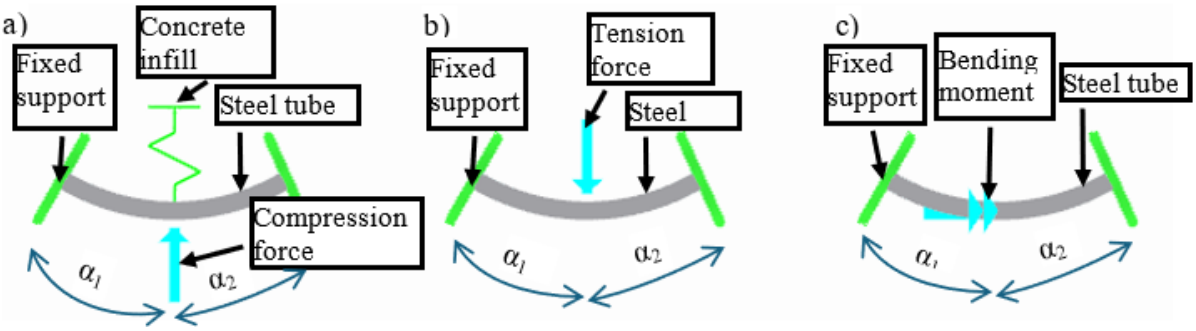

Figure 7: Steel-tube-wall beam model for simulating the steel tube with concrete infill behavior with different loads: a) compression force; b) tensile force; c) bending moment.

For the case of tension and compression forces (Figure 7 a and b), the steel-tube-wall beam model had a statical indeterminacy degree of 3, while for the case of the bending moment being directly transferred to the neighboring interim steel plates, the steel-tube-wall beam model had a statical indeterminacy degree of 2. The concrete infill stiffness was calculated by considering the infill as a beam with varying cross-section width and loaded with an axial force. For the first mechanism, the rotational stiffness was calculated based on equilibrium conditions of forces and moments on a fictitious contact plane between the steel tube and the concrete infill. The two equilibrium equations were used to calculate two unknowns: the compressed height of the steel tube wall and the rotation. The rotational stiffness of the steel tube with concrete infill was calculated as the sum of the rotational stiffnesses of the two considered mechanisms.

For the rotational stiffness of the connection with the glued-in threaded rods, the stiffness of the following elements of the connection was taken into account: steel endplate (as an equivalent T-stub according to Eurocode 3 [12]), bolt head, washer, bolt shaft, bolt and coupling nut threads (statically indeterminate system), coupling nut, threaded rod and coupling nut thread (statically indeterminate system), threaded rod and ordinary nut threads (statically indeterminate system), glued-in part of the threaded rod. For the stiffness of the glued-in threaded rods, the expressions from [13] and [14] were considered (different for compression and tension loading). For the effective shear stiffness (required to calculate the axial or slip stiffness of the glued-in threaded rods), the value from [15] was taken into account (30 N/mm). This value was determined for a threaded rod of the same diameter, timber of similar strength class and similar epoxy adhesive as used in the present study. The basis for this choice is the fact that most of the slippage or displacement of glued-in threaded rods (with stiff adhesives) results in the deformation of the wood layer near the contact surface between the adhesive and the wood. A more accurate value for the effective shear stiffness could only be determined by tensile tests on glued-in threaded rods with different glued-in lengths.

For the compression part of the cross-section (contact between the glulam beam end face and the steel endplate), the compression stress (or force) was considered to be transmitted through the contact between the glulam beam end face and the steel endplate and also to threaded rods in the compression zone. For the stiffness of the steel endplate in the compression zone, the terms for a rigid plate in an elastic half-space (in this case, glued laminated timber, in the direction parallel to the fibers). The expressions used were taken from [16].

It was considered that the load-bearing capacity is limited by the load-bearing capacity of the glued-in threaded rods loaded in tension, which was calculated according to the German national annex to the Eurocode 5 [17], which assumes 4 MPa for the shear strength of the glued-in threaded rod bonds up to glued-in lengths of 250 mm. The calculated characteristic load-bearing capacity of the glued-in rod was 47.25 kN. The mean load-bearing capacity of the glued-in rods (62.17 kN) was calculated by considering the ratio of the characteristic and mean load-bearing capacity of the glued-in threaded rods from [18], equal to 0.76. The model in Figure 8 was used to calculate the rotational stiffness of the connection with glued-in threaded rods and the load-bearing capacity (maximum bending moment with accompanying axial force). Two unknowns were calculated based on the equilibrium of forces and moments in the cross-section (the height of the compression zone and the rotational stiffness).

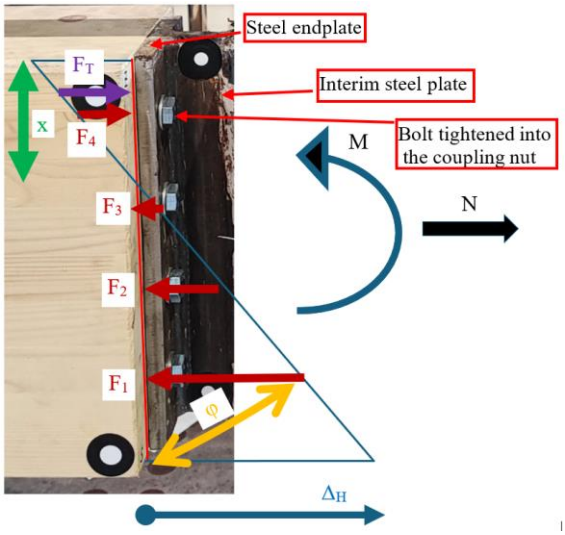

Figure 8: Calculation model for the rotational stiffness and load-bearing capacity of the connection with glued-in threaded rods loaded with a bending moment and an axial force.

The symbol x in the model in Figure 8 denotes the compression zone height, F_i are the glued-in threaded rod forces, F_T is the resultant of the compressive stresses transmitted directly through the contact between the glulam beam end face and the steel endplate, M is the bending moment, N is the axial force, φ is the angle of rotation, Δ_H are the horizontal displacements (perpendicular to the contact plane). The relation between the bending moment and the axial force was calculated from the structural analysis model in Figure 9.

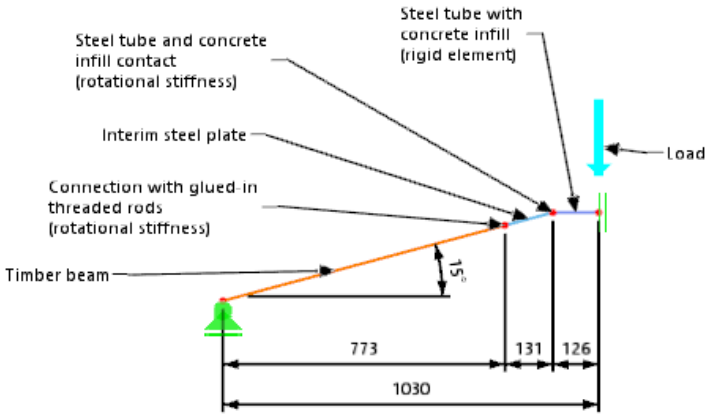

Figure 9: Structural analysis model for calculating the test specimen's inner static quantities and vertical displacement (linear dimensions in mm).

The structural analysis model in Figure 9 assumed that the vertical load is evenly distributed to all six beams connected to the joint with the applicated load. Considering symmetry conditions, only one of the six beams was used in the model. The left-end support in Figure 9 was a sliding support, while the right-end support in Figure 9 restrained horizontal movements and rotations. Axial, shear and flexural deformations of the glulam beam and interim steel plate were considered in addition to the rotational stiffnesses of the connection with glued-in threaded rods and the rotational stiffness of the steel tube and the concrete infill contact to calculate the vertical displacement with the virtual work method. The concrete-infilled steel tube's projected length was considered an infinitely rigid element.

3.3 Calculation results and comparison with the load-bearing test

The stiffness and load-bearing capacity calculation results of the structural analysis model in Figure 9 are given in Table 2. Additionally, some relevant interim results are also given.

Table 2: Calculation results.

Property	Result
Concrete infill axial stiffness (half of the cylinder loaded transversely considered)	15563 kN/mm
Steel tube (without infill) axial stiffness (tension or compression load)	676 kN/mm
Rotational stiffness of the steel tube and concrete infill contact (force couple – first mechanism)	21591 kNm/rad
Rotational stiffness of the steel tube and concrete infill contact (torsion – second mechanism)	527 kNm/rad
Glued-in threaded rod compression axial stiffness	182 kN/mm
Glued-in threaded rod tensile axial stiffness	216 kN/mm
Rotational stiffness of the glued-in threaded rod connection	12827 kNm/rad
Stiffness of the structural analysis model in Figure 9 (ratio of the load and the vertical joint displacement)	**47.4 kN/mm**
Bending capacity of the glued-in threaded rod connection (with accompanying axial force according to the structural analysis model in Figure 9)	39 kNm (-13 kN)
Load-bearing capacity of the specimen according to the structural analysis model in Figure 9	**304 kN**

The comparison of the load-bearing test results in Table 1 and the calculation results in Table 2 shows that the proposed calculation model slightly overestimates the stiffness of the test specimen. In contrast, the calculated load-bearing capacity is lower than the measured load-bearing capacity. It can be concluded that the proposed model for analyzing the test specimen's structural behavior gives acceptable results.

Conclusion

The paper presents a load-bearing test of six glulam beams joined with a hybrid steel-concrete joint for discrete reticulated timber shell structures. The pull-out failure of the glued-in threaded rods limited the load-bearing capacity of the test specimen. Even though the failure of individually tensioned glued-in threaded rods is usually brittle, the test specimen showed ductile behavior, which might be attributed to the configuration of multiple glued-in threaded rods in each of the glulam beams and due to the possibility of redistribution of the load to multiple glulam beams. An important observation was that the load-bearing test did not result in concrete infill damage (no noticeable cracks on the concrete infill visible surfaces).

In addition to the experimental determination of the load-bearing capacity and stiffness of the test specimen, the paper also presents a structural analysis model for calculating the load-bearing capacity and stiffness of the test specimen. The structural analysis model involved the calculation of the rotational stiffness of the glued-in rod connection and the rotational stiffness of the steel tube and concrete infill contact. The model for calculating the rotational stiffness of the glued-in threaded rod connection was a

system of parallel and series springs. In contrast, the model for calculating the rotational stiffness of the steel tube and concrete infill contact was another structural analysis model involving beam elements. The comparison of the experimental and calculated load-bearing and stiffness results indicates the usefulness of the presented calculation model, as the results show reasonable agreement. While the structural analysis model overestimates the specimen's stiffness, the calculated load-bearing capacity was lower than the experimentally observed load-bearing capacity.

Acknowledgments

This research was funded by the Slovenian Research and Innovation Agency (project number Z2-4425).

References

[1] S. H. Dyvik, B. Manum, and A. Rønnquist, "Gridshells in Recent Research—A Systematic Mapping Study," *Applied Sciences*, vol. 11, no. 24, p. 11731, 2021.

[2] B. D'Amico, A. Kermani, and H. Zhang, "Form finding and structural analysis of actively bent timber grid shells," *Engineering Structures*, vol. 81, pp. 195–207, 2014.

[3] M. D. Shivegowda, P. Boonyasopon, S. M. Rangappa, and S. Siengchin, "A Review on Computer-Aided Design and Manufacturing Processes in Design and Architecture," *Archives of Computational Methods in Engineering*, Feb. 2022, doi: 10.1007/s11831-022-09723-w.

[4] M. Bahramian and K. Yetilmezsoy, "Life cycle assessment of the building industry: An overview of two decades of research (1995–2018)," *Energy and Buildings*, vol. 219, p. 109917, Jul. 2020, doi: 10.1016/j.enbuild.2020.109917.

[5] R. Minunno, T. O'Grady, G. M. Morrison, and R. L. Gruner, "Investigating the embodied energy and carbon of buildings: A systematic literature review and meta-analysis of life cycle assessments," *Renewable and Sustainable Energy Reviews*, vol. 143, p. 110935, Jun. 2021, doi: 10.1016/j.rser.2021.110935.

[6] J. O'donnell, H. Sefi, B. Sitler, N. Williams, K. Crolla, and Y.-M. M. Xie, "Smart Nodes Pavilion–Bi-Directional Evolutionary Structural Optimization and Additive Manufacturing," in *Proceedings of IASS Annual Symposia*, International Association for Shell and Spatial Structures (IASS), 2015, pp. 1–12.

[7] M. M. Abdelwahab and K. D. Tsavdaridis, "Optimised 3D Printed Metallic Node-Connections for Reticulated Structures," in *Proceedings of the 9th International Conference on Steel and Aluminium Structures (ICSAS19)*, Independent Publishing Network, 2019, pp. 423–434.

[8] Z. Chen, J. Zhao, H. Liu, S. Zhao, S. Yang, and J. Liu, "Research progress and engineering practice of glulam space frame structures," in *Proceedings of IASS Annual Symposia*, International Association for Shell and Spatial Structures (IASS), 2022, pp. 1–12.

[9] "Leaders in Concrete & Concrete Products: BarChipInc," Barchip, https://barchip.com/product/. Accessed: Nov. 13, 2023. [Online]. Available: https://barchip.com/product/

[10] European Committee for Standardization, "EN 14889-2:2006 Fibres for concrete Polymer fibres. Definitions, specifications and conformity." 2006.

[11] Ž. Unuk and M. Kuhta, "Nonlinear Semi-Numeric and Finite Element Analysis of Three-Point Bending Tests of Notched Polymer Fiber-Reinforced Concrete Prisms," *Applied Sciences*, vol. 14, no. 4, p. 1604, 2024.

[12] European Committee for Standardization., "EN 1993-1-8; Eurocode 3: Design of steel structures — Part 1-8: Design of joints." 2005.

[13] J. L. Jensen, A. Koizumi, T. Sasaki, Y. Tamura, and Y. Iijima, "Axially loaded glued-in hardwood dowels," *Wood science and technology*, vol. 35, pp. 73–83, 2001.

[14] J. L. Jensen, M. Nakatani, P. Quenneville, and B. Walford, "A simple unified model for withdrawal of lag screws and glued-in rods.," *European Journal of Wood and Wood Products*, vol. 69, no. 4, pp. 537–544, 2011.

[15] P. J. Gustafsson and E. Serrano, *Glued-in rods for timber structures: development of a calculation model*. Division of Structural mechanics, Lund University, 2001.

[16] R. V. Whitman and F. E. Richart Jr, "Design procedures for dynamically loaded foundations," *Journal of the Soil Mechanics and Foundations Division*, vol. 93, no. 6, pp. 169–193, 1967.

[17] Normenausschuss Bauwesen (NABau) im DIN, "DIN EN 1995-1-1/NA:2013-08: National Annex – Nationally determined parameters – Eurocode 5: Design of timber structures – Part 1-1: General – Common rules and rules for buildings." 2013.

[18] A. Rossignon and B. Espion, "Experimental assessment of the pull-out strength of single rods bonded in glulam parallel to the grain," *European Journal of Wood and Wood Products*, vol. 66, no. 6, pp. 419–432, 2008.